BIOCHEMISTRY
including biophysical chemistry & molecular biology

Article

pubs.acs.org/biochemistry

Effects of the Oncogenic $V_{664}E$ Mutation on Membrane Insertion, Structure, and Sequence-Dependent Interactions of the Neu Transmembrane Domain in Micelles and Model Membranes: An Integrated Biophysical and Simulation Study

Andrew J. Beevers,[†] Anthony Nash,[‡] Martha Salazar-Cancino,[†] David J. Scott,[∥] Rebecca Notman,[§,†] and Ann M. Dixon*[,†]

[†]Department of Chemistry, [‡]MOAC Doctoral Training Centre, and [§]Centre for Scientific Computing, University of Warwick, Coventry CV4 7AL, U.K.

[∥]Department of Biosciences, University of Nottingham, Nottingham, U.K.

Supporting Information

ABSTRACT: Receptor tyrosine kinases bind ligands such as cytokines, hormones, and growth factors and regulate key cellular processes, including cell division. They are also implicated in the development of many types of cancer. One such example is the Neu receptor tyrosine kinase found in rats (homologous to the human ErbB2 protein), which can undergo a valine to glutamic acid ($V_{664}E$) mutation at the center of its α-helical transmembrane domain. This substitution results in receptor activation and oncogenesis. The molecular basis of this dramatic change in behavior upon introduction of the $V_{664}E$ mutation has been difficult to pin down, with conflicting results reported in the literature. Here we report the first quantitative, thermodynamic analysis of dimerization and biophysical characterization of the rat Neu transmembrane domain and several mutants in a range of chemical environments. These data have allowed us to identify the effects of the $V_{664}E$ mutation in the isolated TM domain with respect to protein−protein and protein−lipid interactions, membrane insertion, and secondary structure. We also report the results from a 100 ns atomistic molecular dynamics simulation of the Neu transmembrane domain in a model membrane bilayer (dipalmitoylphosphatidylcholine). The results from simulation and experiment are in close agreement and suggest that, in the model systems investigated, the $V_{664}E$ mutation leads to a weakening of the TM dimer and a change in sequence-dependent interactions. These results are contrary to recent results obtained in mammalian membranes, and the implications of this are discussed.

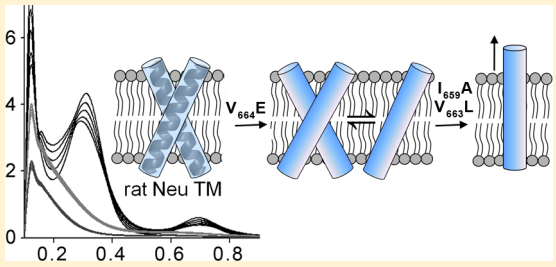

The protein encoded by the rat *neu* proto-oncogene is a membrane-spanning receptor tyrosine kinase (RTK), homologous to the ErbB2 protein in humans, which plays a key role in cell division and cell growth. RTKs are thought to be activated via dimerization of their intracellular tyrosine kinase domain, either as a result of a ligand binding to the N-terminal extracellular domain or by lateral interactions of the transmembrane (TM) domains (as is likely the case for the orphan human ErbB2 receptor), leading to phosphorylation of a tyrosine residue and a subsequent signaling cascade. Neu is vulnerable to a point mutation near the center of its TM domain [$V_{664}E$ (see Figure 1)] that leads to receptor overactivation and oncogenesis.[1−4] The mechanism via which this single-point mutation leads to cancer has been the subject of many studies, as summarized in our recent report,[5] because insight into the molecular basis of the oncogenic effects of this mutation is key to understanding signal transduction for this (and potentially other) RTKs.

Several structural changes are possible upon substitution of a hydrophobic Val residue with a negatively charged Glu residue in the center of a helical TM domain. The $V_{664}E$ mutation in Neu could cause deformation of the peptide backbone (e.g., a change in the secondary structure content of the TM domain)

Neu: RASW*VTFIIATVVGVLLFLILVVVVGILIKRRR
Neu*: RASW*VTFIIATV**E**GVLLFLILVVVVGILIKRRR
NeuQM: RASW*VTF**A**I**L**T**L**V**L**VLLFLILVVVVGILIKRRR
Neu*DM: RASW*VTF**A**IAT**L**VGVLLFLILVVVVGILIKRRR

Figure 1. Sequences of peptides used in this study, including the transmembrane domain of the wild-type (proto-oncogenic) rat Neu protein (Neu) and the transmembrane domain containing the oncogenic $V_{664}E$ mutation (Neu*). Also shown are mutants that lead to significant weakening of helix−helix interactions in *Escherichia coli* membranes for the wild-type TM (specifically $I_{659}A/A_{661}L/V_{663}L/G_{665}L$, NeuQM) and the oncogenic TM ($I_{659}A/V_{663}L$, Neu*DM). For all four peptides, the native Pro_{655} residue was changed to Trp (W* in sequence) to aid in detection of the peptide in analytical ultracentrifugation experiments.

Received: August 11, 2011
Revised: February 28, 2012
Published: March 2, 2012

or change the degree of membrane insertion of this domain. Both of these properties have been studied by us[5] and by others[6−13] for both wild-type Neu and the oncogenic $V_{664}E$ mutant (here denoted Neu*), but the results are conflicting depending on the experimental approach taken. The oncogenic mutation may also change the orientation of the TM helices with respect to the bilayer normal. Fewer studies have provided information about the orientation (i.e., tilt and crossing angles) of the TM helices in Neu and Neu*; however, it has been shown by infrared[12] and linear dichroism[5] spectroscopy that the $V_{664}E$ mutation causes an increase in the tilt angle.

The oncogenic mutation may also alter TM helix−helix interactions, and it is this effect of the $V_{664}E$ mutation that has been most frequently studied. In vivo studies of the Neu TM domain and the related human ErbB2 TM domain in bacterial membranes[5,14] suggest that incorporation of the $V_{664}E$ mutation leads to a slight reduction in the level of TM self-association. However, cross-linking studies performed in mammalian membranes suggest the reverse is true.[15]

In a recent study, we uncovered an additional effect of the $V_{664}E$ mutation on the Neu TM domain, namely that the sequence-dependent mode(s) of helix−helix interaction is altered upon mutation.[5] Our data (obtained in the *Escherichia coli* inner membrane using the TOXCAT assay[16]) suggested that oligomerization of the wild-type Neu TM domain is supported by multiple interaction modes, stabilized (in part) by two highly conserved sequence motifs located on opposite helical faces. These motifs are (i) a motif containing Ala 661 and Gly 665 [$A_{661}XXXG_{665}$ (Figure 1)], known as the Sternberg−Gullick motif[17] and similar to the GXXXG motif seen in many transmembrane α-helical oligomers,[18] and (ii) a motif consisting of $I_{659}XXXV_{663}$ (Figure 1). Mutation of either motif had only a weak effect on self-association, presumably because the other motif remained available for interaction. Conversely, the oncogenic Neu* TM domain appeared to have only one mode of oligomerization stabilized largely by the $I_{659}XXXV_{663}$ motif; mutation of this motif led to a large decrease in the level of self-association, while mutation of the $A_{661}XXXG_{665}$ motif actually strengthened the association.[5]

We interpreted these results in the framework of the "molecular switch" or "rotational coupling" model that has been proposed for Neu and a number of other RTKs.[19−22] In this model, ligand binding (or mutation) causes a conformational change in a preformed, inactive RTK dimer that leads to receptor activation.[23,24] We suggested that the $V_{664}E$ mutation may prevent this conformational change (e.g., by restricting rotation of TM helices about their long axes), effectively locking the receptor in its "active" conformation. This "conformational switch" model exists alongside a more widely accepted model for the mechanism of RTK signaling, specifically one in which activation simply occurs via ligand-induced (or mutation-induced) dimerization, and the inactive form of the protein is predominantly monomeric. Given the strength of oligomerization observed in bacterial membranes using the TOXCAT assay, our previous data for Neu and Neu* best fit the conformational switch model. However, the TOXCAT assay has significant limitations in that it cannot report the oligomeric state, the measurements are taken in the context of a fusion protein whose contributions have not been exhaustively characterized, and the dimerization propensity of the positive control used in the assay (namely the TM domain of glycophorin A) has been called into question in a recent study.[25]

Therefore, it was the aim of this work to ascertain the oligomeric states and report, for the first time, the dissociation constants of the wild-type Neu and Neu* TM domains (as well as two mutants that were found to strongly disrupt self-association in bacterial membranes) to develop a fuller understanding of the effects of the $V_{664}E$ mutation. To achieve this, we used simple model systems comprised of purified peptides derived from the Neu TM domain reconstituted in either detergent micelles or POPC membranes. Analytical ultracentrifugation (AUC) was selected for these studies as it is a primary analytical method that can be used to obtain information about molecular size and shape in a range of chemical environments, including mild detergents that act as membrane mimetics. AUC has the added benefit of providing a thermodynamic description of binding events, as values for binding constants and Gibbs free energy can be extracted from the data. In this way, we were able to report here the overall contribution of TM helix−helix interactions to RTK dimerization for Neu and related mutants. We complemented this work with measurements from a range of biophysical methods to assess the secondary structure and membrane insertion of all TM domains tested. Finally, a 100 ns molecular dynamics (MD) simulation was conducted in a membrane bilayer for the $I_{659}XXXV_{663}$ putative interaction mode thought to stabilize the wild-type TM dimer. Our results were in close agreement with previous results obtained in the *E. coli* inner membrane using TOXCAT[5] and were interpreted in light of current models for RTK activation.

MATERIALS AND METHODS

Synthesis and Purification of Transmembrane Domain Peptides. Peptides were synthesized using solid-phase FMOC chemistry at the W.M. Keck Biotechnology Resource Laboratory, New Haven, CT. Four peptides were prepared, containing sequences derived from the transmembrane domains of the wild-type (proto-oncogenic) rat Neu protein (R_{652}ASWVTFIIATVVGVLLFLILVVVVGILIKRRR$_{684}$; MW = 3721.7 Da), the oncogenic Neu* protein containing the $V_{664}E$ mutation in the wild-type sequence (MW = 3751.6 Da), and two selectively mutated sequences that resulted in significant weakening of helix−helix interactions as reported previously using the TOXCAT assay[5] [namely, Neu $I_{659}A/A_{661}L/V_{663}L/G_{665}L$ or Neu_{QM} (MW = 3791.8 Da) and Neu* $I_{659}A/V_{663}L$ or Neu^*_{DM} (MW = 3723.6 Da)]. In each case, the native Pro_{655} residue was mutated to Trp to yield significant absorbance at 280 nm, which was in turn used to determine protein concentration and monitor protein sedimentation using AUC. Peptide concentrations were estimated from the absorbance at 280 nm using a molar extinction coefficient (ε_{280}) of 5500 mol^{-1} cm^{-1} for all four peptides. Each peptide was purified using reversed-phase high-performance liquid chromatography and a Jupiter C4 column (Phenomenex, Macclesfield, U.K.) with a linear gradient of 2-propanol (30 to 100%) as the mobile phase. The purity of fractions was confirmed using electrospray ionization time-of-flight (ESI-TOF) mass spectrometry (Bruker, Coventry, U.K.), and all pure fractions were pooled, lyophilized, and stored as dry powders until they were used.

Preparation of Proteoliposomes. Purified peptides were cosolubilized with palmitoyloleoylphosphocholine (POPC) (Avanti Polar Lipids, Alabaster, AL) in trifluoroethanol (TFE) at a peptide:lipid molar ratio of 1:30 for Fourier transform infrared (FTIR) analyses and a peptide:lipid mass ratio of 1:10 for circular dichroism (CD) analyses. TFE was then removed using rotary evaporation under vacuum. The resulting lipid−peptide films were then resuspended in either (i) water to a final peptide concentration of 10 mg/mL (adjusted to pH 7.4) for FTIR

dx.doi.org/10.1021/bi201269w | *Biochemistry* 2012, 51, 2558−2568

analyses or (ii) 50 mM Tris buffer (pH 7.4) to a final peptide concentration of 2.5 mg/mL for CD analyses. The resulting mixtures were sonicated and subjected to three freeze−thaw cycles using liquid nitrogen. Finally, in the case of CD samples, the solution was extruded through a 100 nm polycarbonate membrane.

Circular Dichroism Spectroscopy. All CD spectra were recorded on a Jasco J600 spectrophotometer using a 1 mm path-length quartz cuvette (Starna, Optiglass Ltd., Hainault, U.K.). Spectra were recorded as an average of 16 scans in the wavelength range of 190−300 nm. Spectra were collected for proteoliposome samples (described above) as well as samples containing peptide dissolved in TFE or 50 mM Tris (pH 7.4), containing 15 mM dodecylphosphocholine detergent (DPC) (Avanti Polar Lipids) and 100 mM NaCl. Both TFE and detergent samples were prepared with a final peptide concentration of 100 μM, as determined by UV−vis spectroscopy. An equivalent CD spectrum of either TFE, DPC micelles, or POPC vesicles recorded in the absence of peptide was subtracted to obtain the final spectra shown.

Infrared Spectroscopy. Proteoliposome samples (100 μL) were deposited onto a trapezoidal zinc selenide (ZnSe) crystal (Specac, Orpington, Kent, U.K.) and dried under a stream of diffused nitrogen gas to produce a bilayer film. Attenuated total reflectance Fourier transform infrared (ATR-FTIR) spectra were then recorded as an average of 1000 interferograms collected between 4000 and 1000 cm^{-1}, with a resolution of 4 cm^{-1}, using a Jasco FTIR-470 spectrometer equipped with a liquid nitrogen-cooled MCT detector purged with a continuous stream of dried compressed air. For the deuterium exchange measurements, a stream of nitrogen was saturated with D_2O and passed over the bilayer film using a top flow-through plate (Specac, Orpington, Kent, U.K.). Spectra were then recorded after exposure of the samples to D_2O for 1 and 22 h. Amide I and amide II bands in the initial and both D_2O-exposed spectra were integrated using OriginPro version 8.1, and the ratio of the amide II to amide I peak areas was calculated for each spectrum to account for sample swelling that can occur following D_2O exposure, lowering the magnitude of the overall absorbance signal as described previously.[5] The degree of membrane insertion was determined by comparing these values for spectra before and after D_2O exposure. Fourier self-deconvolution[26] of the amide I region of the spectrum followed by peak fitting (performed using GRAMS/AI, Thermo Scientific) was performed as described previously[27] to obtain the secondary structure content of each peptide.

Analytical Ultracentrifugation. Sedimentation equilibrium and sedimentation velocity measurements were taken on a Beckman-Coulter XL-A analytical ultracentrifuge (Beckman Coulter, Fullerton, CA) housed in the Department of Biosciences of the University of Nottingham. All peptides were solubilized in 50 mM Tris (pH 7.4), containing 15 mM DPC, 100 mM NaCl, and 52.5% D_2O (Cambridge Isotope Laboratories, Andover, MA) to match the buoyant density of the detergent. All data were collected at a set temperature of 20 °C using absorbance optics set to 280 nm. For sedimentation equilibrium measurements, a six-channel centerpiece was used (Spin Analytical, Berwick, ME). Measurements were taken at one peptide concentration (150 μM) and three speeds (48000, 55000, and 60000 rpm). Samples were centrifuged for time periods in excess of those required to reach equilibrium (22 h per speed), and the establishment of sedimentation equilibrium was verified using WinMatch to subtract successive scans until no difference was observed. The monomeric molecular masses and partial specific volumes of the Neu peptides in 52.5% D_2O (corrected for H−D exchange) were determined using SEDNTERP[28] available at http://ww.rasmb.bbri.org/. Global fitting of the three data sets was performed using WinNONLIN[29] to conduct nonlinear least-squares curve fitting as described previously.[30] The goodness of fit of data to a particular model was judged by the spread of the residuals around the best fit and minimization of variance. The molar association constant for a monomer−dimer equilibrium (k_{1-2}), the apparent free energy of dissociation (ΔG_{app}), and the mole fraction standard state free energy of dissociation ($\Delta G°_{x}$, which accounts for detergent concentration) were calculated as described previously.[30]

Sedimentation velocity data were collected at peptide concentrations of 38, 76, and 152 μM. Samples were loaded into two-channel sedimentation velocity cells containing SedVel60K centerpieces (Spin Analytical, Berwick, ME) and analyzed at 60000 rpm. Cells were scanned radially every 5 min. Data were analyzed using SEDFIT[31] and sedimentation coefficient distributions derived using the $c(S)$ algorithm. Data were then subjected to 1000 runs of a Monte Carlo routine to determine the extent of error in the distributions. The buffer density was the same as that used for the equilibrium experiments, and the buffer viscosity was measured as 1.162 cP.

Molecular Dynamics Simulations. Atomistic-level MD simulations were conducted for a pair of identical wild-type Neu transmembrane peptide sequences (R_{652}−R_{684}), inserted as a dimer into a single-component dipalmitoylphosphatidylcholine (DPPC) lipid bilayer in aqueous solution. The simulation system consisted of 180 DPPC lipids, 20171 water molecules, and 10 chloride counterions. To generate a starting structure for the dimer in which the $I_{659}XXXV_{663}$ motif forms the primary binding interface, we subjected the Neu sequence to a global conformational search in vacuum using the CHI algorithm.[32] The experimental details of this search are given in the Supporting Information, and the starting structure is shown in Figure S3 of the Supporting Information. The DPPC bilayer was created by aligning a single DPPC molecule along the z-direction and then replicating the molecule in the x- and y-directions to form a monolayer. The monolayer was then replicated and rotated to yield a bilayer structure. The bilayer was solvated with water and then subjected to MD simulation for 4 ns in the *NVT* ensemble followed by MD simulation for 10 ns in the *NPT* ensemble (specific details of the simulation parameters used are given in the Supporting Information). Following equilibration, the selected Neu complex was inserted into the center of the bilayer and any overlapping DPPC lipid molecules were removed. The Neu protein bilayer system also required a careful equilibration procedure to ensure that the initial structure of the Neu complex was not perturbed far from its starting configuration while the bilayer re-equilibrated. The equilibration steps are summarized in the Supporting Information. Following equilibration, all position restraints were switched off and the peptide−DPPC system was simulated for 100 ns.

The helicity of each residue was determined using the g_helix tool supplied with GROMACS, whereby the helicity is computed from the rmsd of the backbone ϕ and ψ angles from those of an ideal α-helix. The crossing point distance was computed by minimizing the point of approach between the interhelical Cα atoms along the principal axis of two helices, which is the approach outlined by Chothia et al.[33] The distance between the two peptides is recorded once the derivative of the closest approach is equal to zero. The tilt angle of a helix as a function of time was computed from the dot product between

the axis normal to the bilayer and the principal axis of the helix. The principal axis is defined as the eigenvector whose corresponding eigenvalue is the smallest from the inertia tensor matrix of that helices' Cα atoms.[33]

RESULTS

Neu and Neu* Are Both Highly Dimeric in DPC Detergent Micelles, but the Oncogenic Point Mutation Reduces the Strength of Dimerization by 1.1 kcal/mol. Our previously reported TOXCAT data could not report on the oligomeric states of the Neu and Neu* TM domain,[5] yet an understanding of this property is critical to fully interpret the effects of the $V_{664}E$ mutation as well as the additional disruptive mutations. Thus far, the method used almost exclusively to determine the oligomeric states of Neu and Neu* TM domains in vivo and in vitro is SDS−PAGE.[7,8,15,34] We have also used SDS−PAGE in previous studies of the Neu TM, but the results were in conflict with results obtained in bacterial membranes.[5] In the *E. coli* inner membrane, we observed a reduction in the level of TM self-association upon introduction of the $V_{664}E$ mutation; however, no difference in homo-oligomerization was observed when TM peptides were analyzed using SDS−PAGE (both peptides migrated identically as ~6 kDa species). It is becoming well-known that transmembrane proteins can migrate anomalously during SDS−PAGE analyses because of strong binding of detergent to the protein,[35] increasing the effective mass and complicating interpretation of the data for smaller proteins. In some cases, it could be impossible to distinguish dimers from denatured monomers carrying a significant amount of bound detergent. When an alternative method (namely analytical ultracentrifugation) was used to study TM domain oligomerization for a closely related receptor tyrosine kinase, human ErbB2, the TM domain was found to form weak trimers in a non-SDS environment.[36] The anomalous results we obtained using SDS−PAGE,[5] especially when compared to measurements of TM helix association for Neu and Neu* in bacterial membranes,[5,14] led us to use analytical ultracentrifugation in this study to investigate the oligomeric states of peptides derived from the TM domains of Neu and Neu*. AUC is a primary biophysical method, providing data that can be directly related to molecular mass (i.e., interpretation of data does not require use of a potentially inappropriate molecular mass standard). It has a further benefit in that data can be collected under relatively mild conditions (as compared to SDS−PAGE). Membrane proteins solubilized in the neutral detergent C_8E_5[37] and the zwitterionic detergent DPC[30,38] have been successfully analyzed using AUC to yield molecular mass distributions that agree well with data obtained in membrane bilayers.

The AUC instrument used in this work required monitoring of protein absorbance; however, the native sequence of the Neu TM and juxtamembrane domains contained within our peptides contained no selective chromophore (i.e., no Trp residue) and only absorbed light at a wavelength of 220 nm (where the chances of interference from other buffer components are increased). Therefore, in this work, we added a Trp residue in place of the native Pro residue at position 655 (Figure 1). This Pro to Trp mutation had very little effect on the helicity (Figure S1 of the Supporting Information) or membrane insertion (discussed later) of the Neu TM domain peptides and greatly facilitated collection of AUC data.

Both sedimentation equilibrium and sedimentation velocity experiments were employed in this study. Used together, these two methods provide complementary information about the size and shape of protein complexes as well as the thermodynamic parameters that define the strength of interaction (i.e., the apparent molar dissociation constant, K_{app}, and the Gibbs free energy, ΔG). Sedimentation velocity (SV) analyses were conducted for the Neu and Neu* TM peptides at three concentrations (38, 76, and 152 μM) solubilized in DPC-containing buffer using a spinning speed of 60000 rpm. This speed was sufficient to minimize the rate of back diffusion of these small peptides and produce data with the required mass resolution. Sedimentation profiles for Neu and Neu* TM peptides are shown in panels A and B of Figure 2, respectively,

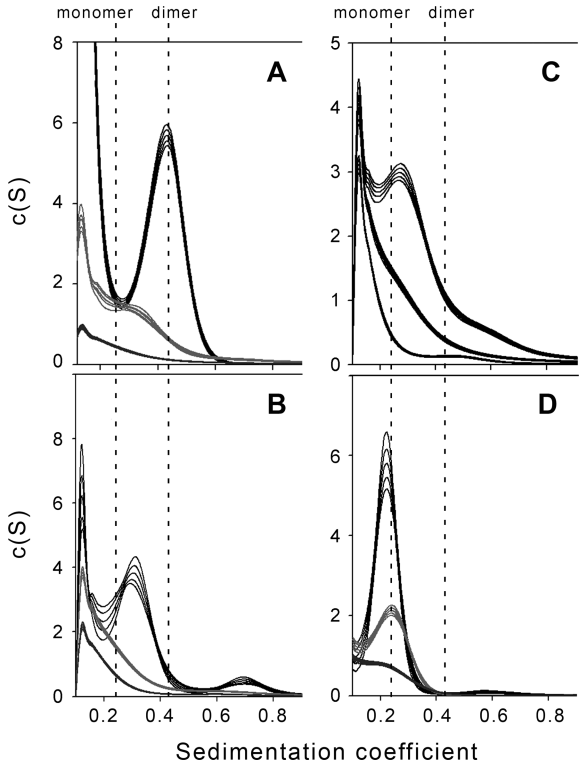

Figure 2. Sedimentation velocity analyses of (A) wild-type Neu, (B) Neu*, (C) Neu^*_{DM}, and (D) Neu_{QM} peptides in a DPC detergent solution at 20 °C. In all cases, analyses were conducted with samples containing 38, 76, and 152 μM peptide. Sedimentation coefficient distribution profiles are shown for each peptide at concentrations of 38 μM (bottom lines), 76 μM (middle lines), and 152 μM (top lines). Conversion of sedimentation coefficients to molecular mass yielded one predominant species in each sample at the highest peptide concentration, and these are compared to theoretical values for the monomer and dimer as indicated by the dashed lines.

with the fit data corresponding to an rmsd of 7.12×10^{-3}. At the highest concentration, the resulting sedimentation coefficient profile for the Neu peptide contains a single species centered at S = 0.43, corresponding to the molecular mass of the peptide dimer (7.4 kDa). The sedimentation coefficient profile for the Neu* peptide contains a single species centered at S = 0.29 corresponding to a molecular mass intermediate between that of the dimer and that of the monomer (monomer mass of 3.8 kDa). At the two lower concentrations, both peptides yielded data that were increasingly difficult to quantify as they produced broad distributions.

Sedimentation equilibrium (SE) analyses were conducted for the Neu and Neu* TM peptides at three speeds and one

dx.doi.org/10.1021/bi201269w | *Biochemistry* 2012, 51, 2558−2568

concentration (the concentration that produced the best data in SV analyses, 150 μM) in DPC detergent micelles, and the concentration versus radial distance profiles at each speed are shown in panels A and B of Figure 3, respectively. The data

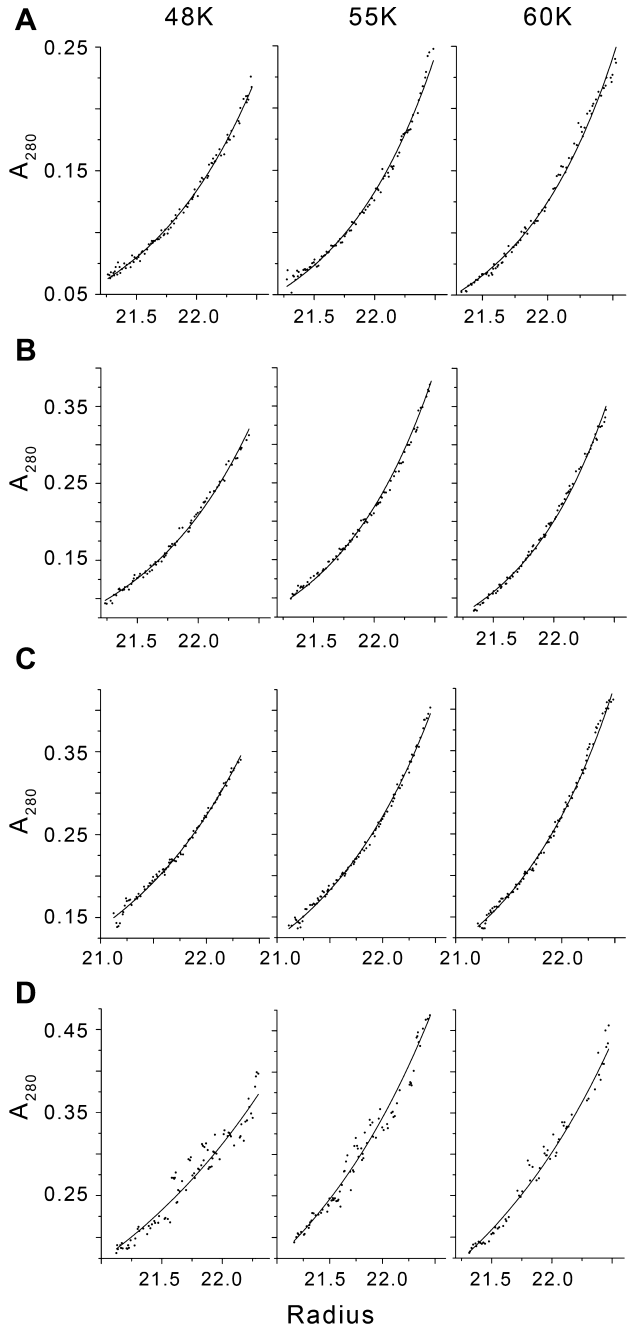

Figure 3. Sedimentation equilibrium analyses of (A) wild-type Neu, (B) Neu*, (C) Neu_{QM}, and (D) $Neu*_{DM}$ peptides in a DPC detergent solution at 20 °C. Three plots are shown for each peptide, corresponding to data collected at one peptide concentration (150 μM) and three speeds (48000, 55000, and 60000 rpm). The filled circles represent the experimental measurements of absorbance at 280 nm, and the solid curves display the best fit resulting from global analysis of all three data sets. Data shown in panels A–C fit best to a model describing a monomer–dimer equilibrium, while data in panel D were best described by a model containing only free monomer.

were first fit to a monomer model, followed by fitting to models of increasing complexity as described previously.[39] The model of best fit was selected on the basis of minimization of the square root of variance (SRV) of the fit and distribution of the fit residuals about zero. In both cases, fitting of the data to a monomer–dimer model resulted in a minimal value for the SRV and the most random fit residuals (not shown). Analyses of the monomer–dimer fits of both peptides yielded apparent monomer–dimer association constants ($k_{1-2\ conc}$), from which the apparent molar dissociation constants (K_{app}) were calculated (see Materials and Methods). Table 1 summarizes the

Table 1. Dimeric K_{app} and Free Energy Calculations for All Four Peptides, Determined from Sedimentation Equilibrium Experiments[a]

	Neu	Neu*	Neu QM	Neu* DM
K_{app} (μM)	1.01	7.20	134	–
ΔG_{app} (kcal/mol)	8.02	6.90	5.19	–
ΔG°_{x} (kcal/mol)	5.53	4.41	2.71	–

[a]There are no values for the Neu* DM peptide, as this peptide was monomeric at all concentrations.

dissociation constants calculated from the data. The Neu peptide yielded a K_{app} of 1.01 μM for the monomer–dimer equilibrium in 15 mM DPC, and the Neu* peptide yielded a slightly higher K_{app} of 7.20 μM. The corresponding values for the standard state free energies of dissociation (ΔG°_{x}) were 5.53 and 4.41 kcal/mol (20 °C) for Neu and Neu*, respectively. These values compare favorably to those obtained using AUC for other TM peptide homodimers, namely, the E5 protein (5.0 kcal/mol)[30] and glycophorin A (7.0 kcal/mol),[40] as well as the K_d and ΔG° values for homodimerization of the closely related HER2 receptor TM domain obtained using FRET (K_d = 2 μM, and ΔG° = 32.3 kJ/mol or 7.7 kcal/mol).[41] The data reported here from SE and SV experiments are also in excellent agreement with analogous measurements taken in the *E. coli* inner membrane using the TOXCAT assay[5] and provide evidence that, in isolation, both the Neu and Neu* TM domains form strong homodimers, and that the oncogenic mutation reduces the strength of the TM homodimer by 1.1 kcal/mol under these conditions.

Mutations Shown To Disrupt Neu and Neu* Dimers in Bacterial Membranes Yield Increasingly Monomeric TM Helices in Micellar Systems. In a previous study, we identified two mutants that strongly disrupted oligomerization of the Neu and Neu* TM domains in the inner membrane of *E. coli*.[5] We found that simultaneous mutation of the two primary helix–helix interaction motifs, $I_{659}XXXV_{663}$ and $A_{661}XXXG_{665}$ (to create the Neu $I_{659}A/A_{661}L/V_{663}L/G_{665}L$ quadruple mutant or Neu_{QM}), was necessary to significantly impact the oligomerization of the wild-type Neu TM domain. Interestingly, mutation of only one of these motifs, $I_{659}XXXV_{663}$ (to create the Neu* $I_{659}A/V_{663}L$ double mutant or $Neu*_{DM}$), was necessary to significantly disrupt oligomerization of the Neu* TM domain. These results were interpreted for Neu and Neu* TM dimers using the conformational switching or flexible rotation model suggested for other RTKs. Confidence in the dimeric nature of both Neu and Neu* TM domains, as provided by the data reported here, provided a strong foundation upon which we could build a thermodynamic description of the effects of these mutations.

Two peptides that contained the mutations described above were prepared [$Neu*_{DM}$ and Neu_{QM} (see Materials and Methods)]. The secondary structure and membrane insertion

dx.doi.org/10.1021/bi201269w | *Biochemistry* 2012, 51, 2558–2568

properties of these peptides were characterized using circular dichroism spectrophotometry (CD) and attenuated total reflection Fourier transform infrared spectroscopy (ATR-FTIR) as before. This was necessary to fully understand the structural impact of the mutations before measurement of any changes in protein−protein interactions. CD spectra for Neu*$_{DM}$ and Neu$_{QM}$ TM peptides, alongside the corresponding spectra of Neu and Neu* TM peptides, in DPC micelles and POPC vesicles are shown in panels A and B of Figure 4, respectively. As observed previously for Neu and Neu* TM peptides solubilized in DMPC vesicles,[5] the spectra for all four peptides are very similar in both shape and intensity and display the characteristic negative maxima at 208 and 220 nm indicative of a predominantly α-helical structure. Although small changes are observed in the magnitudes of the CD signals for the four peptides in a given membrane mimetic, significant light scattering at wavelengths below 200 nm prevented accurate fitting of the data and subsequent quantification of the changes in secondary structure. The similarity of the CD spectra suggests that none of the mutants studied caused significant changes in the secondary structure of the Neu TM domain, but the trend in helicity is as follows: in DPC, helical character follows the trend Neu$_{QM}$ > Neu > Neu*$_{DM}$ > Neu*; in POPC, helical content decreases along the series Neu > Neu$_{QM}$ > Neu*$_{DM}$ > Neu*. These trends largely agree except for the relative helicity of wild-type Neu and the quadruple mutant of this peptide.

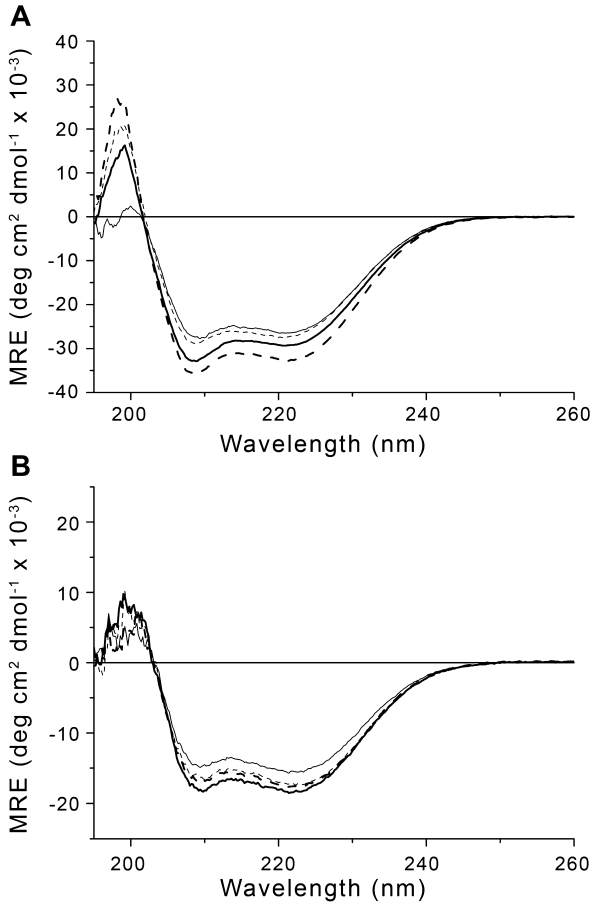

Figure 4. Circular dichroism spectra of wild-type Neu (thick solid line), Neu* (thin solid line), Neu$_{QM}$ (thick dashed line), and Neu*$_{DM}$ (thin dashed line) recorded in DPC detergent micelles (A) and POPC vesicles (B). Data are given in units of mean residue ellipticity (MRE).

Fourier transform infrared (FTIR) measurements were used to assess more quantitatively the helical content of each of the peptides in POPC bilayers. As shown in Figure 5 (solid lines) and Table S1 of the Supporting Information, a Gaussian amide I band (carbonyl stretching) with a maximal frequency of 1655−1656 cm^{-1} was observed in all four spectra. Amide I bands near 1656 cm^{-1} are characteristic of α-helical secondary structure.[42] The amide I region of each spectrum was also subjected to Fourier self-deconvolution[26] followed by fitting of the resulting band to Gaussian curves to quantify secondary structure content. Eight separate curves were needed to accurately fit each of the amide I bands (Figure S2 of the Supporting Information). These bands were assigned on the basis of data from previous studies[27,43] and are summarized in Table 2. If the area of the curves centered at 1655 and 1667 cm^{-1} (α-I-helix and α-II-helix/3-10-helix, respectively[43]) are combined, all peptides have a helical content ranging from 64 to 67%, suggesting there is very little difference in the helicity of the four peptides in POPC. From analysis of the FTIR data, the percent helicity decreases as follows: Neu > Neu$_{QM}$ > Neu*$_{DM}$ > Neu*. This is in exact agreement with the trend obtained in POPC using solution state CD measurements.

Attenuated total reflectance FTIR (ATR-FTIR) was also used to measure changes in membrane insertion upon introduction of the double and quadruple mutations. This was conducted using deuterium exchange measurements, in which ATR-FTIR spectra are collected before and after exposure of the samples to D_2O-saturated nitrogen gas. Amide hydrogen atoms can exchange with deuterium if they are unprotected, such as if they were in an unfolded, flexible region of the peptide and/or a solvent-exposed

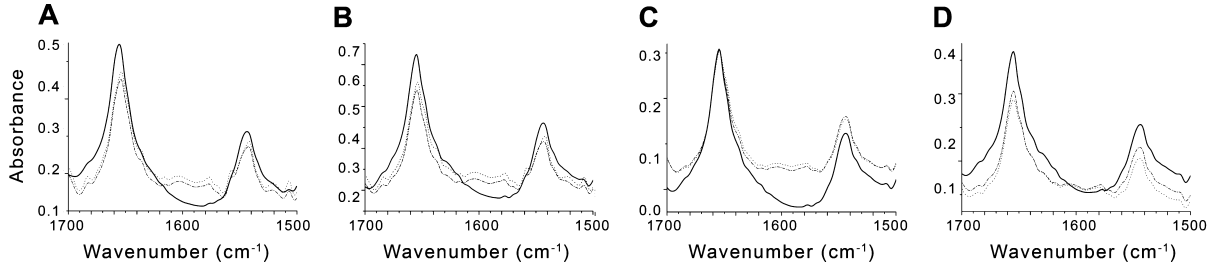

Figure 5. ATR-FTIR spectra of (A) wild-type Neu, (B) Neu*, (C) Neu$_{QM}$, and (D) Neu*$_{DM}$ peptides reconstituted into POPC vesicles. Peptide-loaded POPC vesicles were prepared with a 1:30 (w/w) peptide:POPC ratio. Spectra were acquired before (—), 1 h after (−·−), and 22 h after (···) exposure to D_2O-saturated nitrogen. The positions of the amide I and amide II bands indicate an α-helical secondary structure for all peptides. The spectra remain relatively unchanged after exposure to deuterium, indicating that all of the peptides are predominantly inserted across the bilayer in a transmembrane orientation.

dx.doi.org/10.1021/bi201269w | *Biochemistry* 2012, 51, 2558−2568

Table 2. Secondary Structure Content of Neu TM Peptides in POPC Vesicles Determined Using GRAMS AI To Fit the Amide I Band to Gaussian Curves[a]

frequency of the amide I component (cm^{-1})	assignment	Neu (%)	Neu* (%)	Neu* DM (%)	Neu QM (%)
1685	β-sheet, β-turn	1.9	3.1	2.6	2.5
1677	β-sheet, β-turn, γ-turn	3.4	3.3	3.7	3.3
1667	α-II-helix, 3-10-helix	9.5	11.6	9.9	10.0
1655	α-I-helix	57.9	52.6	56.2	56.4
1644	disordered (irregular)	13.7	15.0	11.4	11.0
1636	β-sheet	6.5	5.3	5.2	8.3
1627	disordered	5.4	5.6	8.6	5.7
1618	disordered	1.6	3.5	2.4	2.8

[a]Bands were assigned on the basis of published values.[28,41]

region lying outside of the membrane bilayer. This exchange leads to a shift in the frequency of the amide II band (N−H bending) due to the increase in the mass of deuterium versus that of hydrogen. Therefore, any change in the magnitude of the amide II band upon exposure to deuterium would suggest exposure of the peptide outside of the bilayer and/or a change in fold. The FTIR spectra of the Neu^*_{DM} and Neu_{QM} peptides reconstituted into POPC bilayers, as well as corresponding spectra for Neu and Neu* peptides, acquired 1 and 22 h after exposure to D_2O are shown in Figure 5 (dotted lines). The area of the amide II band [normalized to that of the amide I band to account for sample swelling (see Materials and Methods)] in each of the peptide samples is given in Table 3. Full details of the positions and areas of the amide I and amide II bands are given in Table S1 of the Supporting Information. Comparison of the

Table 3. Ratios of the Integration Values for the Areas under the Amide I and Amide II Bands for All Peptides and Percentages of Insertion into the Membrane[a]

	Neu	Neu*	Neu QM	Neu* DM
$A_{amide\ II}$:$A_{amide\ I}$ ratio (R)				
initial	0.316	0.302	0.268	0.291
22 h after HDX	0.309	0.305	0.259	0.244
$R_{22\ h}/R_{initial}$	0.977	0.101	0.967	0.837
% exchange	2.3%	0%	3.3%	16.3%

[a]Full integrals are given in Table S1 of the Supporting Information.

normalized area of the amide II band before and after exposure to D_2O indicates that the Neu, Neu_{QM}, and Neu* peptides are well-protected from deuterium exchange, with only 2.3, 3.3, and 0% of the backbone amide groups exchanging, respectively, after 22 h. This would suggest that all three peptides were inaccessible to the aqueous environment (i.e., buried inside, or tightly associated with, the lipid membrane), and none of the mutations lead to a detectable change in insertion. This is in agreement with our previous HDX results[5] that demonstrated both Neu and Neu* TM peptides (containing the native Pro_{655}) were completely protected from exchange in DMPC bilayers, further assuring that the Trp_{655} substitution used in this work was not altering membrane insertion of the TM peptides. However, the Neu^*_{DM} peptide showed markedly different behavior compared to that of the other three, with evidence of significant deuterium exchange for 16.3% of N−H protons (Table 3).

AUC experiments were then used to measure oligomerization of the Neu_{QM} and Neu^*_{DM} TM peptides. SV analyses were conducted at three peptide concentrations as described above, and the sedimentation profiles are shown in panels C and D of Figure 2 for Neu^*_{DM} and Neu_{QM} TM peptides, respectively. The fit data corresponded to an rmsd of 9.75×10^{-3}. As before, data collected at the two lowest concentrations produced broad distributions, while data at the highest concentrations were readily interpreted, resulting in a single species in both sedimentation coefficient profiles. The primary Neu^*_{DM} species had a sedimentation coefficient S of 0.27, intermediate between the expected values for monomer and dimer, but closer to the monomer value. The Neu_{QM} species had a sedimentation coefficient very close to that expected for the monomeric peptide ($S = 0.21$). SE analyses were also conducted as described above, and the concentration versus radial distance profiles at each speed are shown for the Neu_{QM} and Neu^*_{DM} peptides in panels C and D of Figure 3, respectively. Data for the Neu_{QM} peptide fit best to a monomer−dimer model, yielding a K_{app} of 134 μM and a ΔG°_x of 2.71 kcal/mol [20 °C (Table 1)]. This value suggests significant weakening (but not abolishment) of the Neu TM dimer by 2.82 kcal/mol upon mutation of both helix−helix interaction motifs. The data for the Neu^*_{DM} peptide fit best to a monomer model; incorporation of any higher-order oligomeric species led to a sharp decrease in the quality of the fit. Although the results from SE and SV experiments are not in exact agreement regarding the relative propensity of these two peptides to self-associate, both experiments suggest a severe weakening of Neu and Neu* TM homodimers upon mutation of one or both key helix-packing motifs. In general, these results agree well with our recent measurements of homo-oligomerization of these sequences in the *E. coli* inner membrane,[5] in which the Neu^*_{DM} TM domain displayed the weakest propensity to self-associate.

Molecular Dynamics Simulation of the Wild-Type Neu Dimer in a Membrane Bilayer Agrees Well with Experiment. MD simulation is a powerful computational tool that can reveal the interactions of peptides and proteins with lipid bilayer membranes at the molecular level.[44] Until now, modeling studies of the Neu or ErbB TM domain have consisted of conformational searches in vacuum followed by short (<5 ns) MD simulations in vacuum[45] or in dimyristoylphosphatidylcholine (DMPC) lipid bilayers.[46,47] Here, we present the first 100 ns atomistic MD simulation of a wild-type, helical Neu TM domain dimer in a DPPC lipid bilayer in water. A DPPC bilayer was selected because DPPC has been extensively studied by MD simulation using this parameter set and therefore provides a good benchmark system for modeling TM helical peptides. We chose a starting configuration (Figure S3 of the Supporting Information) in which the TM peptides were interacting via the $I_{659}XXXV_{663}$ interface, which is thought to be important for stabilizing dimers of wild-type Neu and the oncogenic form of the protein, Neu*.[5,6] Our simulations were run for >100 ns, and the results demonstrate that it is necessary to access such time scales for key properties such as the position of the protein in the bilayer, helicity, and tilt angle to equilibrate. A snapshot of the system at the end of the simulation is presented in Figure 6A.

Visual inspection of the simulation trajectory reveals that the dimer is located within the bilayer for the duration of the simulation and that the two peptides remain as a dimer, with, at any one time, several interhelical residue−residue contacts

dx.doi.org/10.1021/bi201269w | Biochemistry 2012, 51, 2558−2568

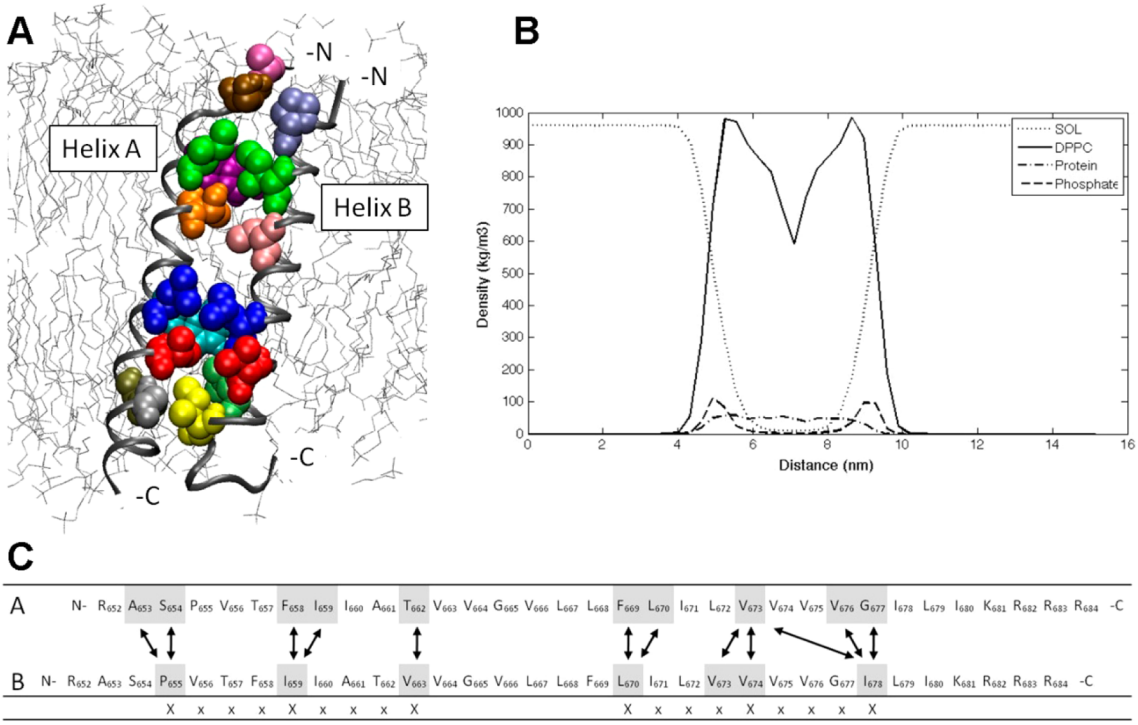

Figure 6. (A) Snapshot of the Neu dimer after MD simulation for 100 ns, which highlights the interacting residues at the binding interface (see panel C for more details and identification of residues). (B) Density profiles of the components of the Neu protein in a hydrated DPPC lipid bilayer as a function of the distance along the bilayer normal. (C) Primary sequence of Neu peptides, with residues that are within 0.8 nm of any other residue shaded in gray. The arrows indicate the specific residue−residue interactions. The XxxxXxxxX motifs are highlighted in the final row.

occurring along the length of the complex. The *z*-height of the dimer rapidly shifts toward its equilibrium position close to the center of the bilayer (Figure S4 of the Supporting Information). The bilayer density profile, shown in Figure 6B, confirms that almost all of the protein is located in the hydrocarbon region of the bilayer with part of the protein extending into the interfacial region. The peptide adopts a tilt angle of ∼24° to deal with any hydrophobic−hydrophilic mismatch in the system.

We observed that the hydrophobic region of the dimer remained in a helical configuration located within the hydrophobic core of the bilayer. The N- and C-terminal residues unfold from the helical starting structure and reside in the headgroup region of the bilayer where they are shielded from the bulk water. The total percentage helicity of the Neu dimer (averaged over all 66 residues) as a function of time is shown in Figure S5 of the Supporting Information. The percentage helicity decreases over the 100 ns until it reaches a value of ∼60%, which is in good agreement with our experimental data obtained from FTIR (cf. ∼67%). The decrease in helicity is due to the ends of the peptides unfolding during the simulation, as shown in Figure 6A. For example, at the N-terminus, the proline acts as a helix breaker, and at the C-terminus, residues K_{681}−R_{684} of both helices are essentially nonhelical while residues G_{677}−I_{680} are less helical. These "unfolded" segments of the peptide lie in the hydrophilic headgroup region of the bilayer. It should be noted that, although the steady decrease in helicity for the entire system (Figure S5 of the Supporting Information) suggests that the system had not fully equilibrated, the percentage helicity of the central segment of the peptides does not change significantly over time, indicating that this region of the peptide forms a stable helix (Figure S6 of the Supporting Information).

The simulations also confirm that the Neu TM peptides form a stable dimer in DPPC lipid bilayers, with the centers of each helix remaining within 1.2 nm of each other for the majority of the simulation time [calculated at the point of crossing (Figure S7 of the Supporting Information)]. The shortest distance between the centers of mass for each reside in one peptide chain and each residue in the other peptide chain is illustrated in Figure S8 of the Supporting Information. Over the course of the simulation, the peptides in the dimer undergo a small rotation from their idealized starting position [i.e., the $I_{659}XXXV_{663}$ interface (Figure S3 of the Supporting Information)] to a dimerization interface characterized by two motifs: $S_{654}XXXF_{658}$-$XXXT_{662}$ ↔ $P_{655}XXXI_{659}XXXV_{663}$ and $F_{669}XXXV_{673}XXXG_{677}$ ↔ $L_{670}XXXV_{674}XXXI_{678}$ (Figure 6A,C). To achieve stabilization via these two motifs, the I_{659}−I_{659} and V_{663}−V_{663} distances (between their centers of mass) in the two helices increase from 3.53 and 4.10 Å to 4.51 and 6.72 Å, respectively. The second (more C-terminal) binding motif could explain the residual association in the quadruple mutant, which was observed by AUC. These MD results agree well with the experimental data presented here for the wt Neu TM domain in micellar and model membrane environments in that they describe stable insertion of the peptide across both leaflets of a membrane bilayer, tight association with the hydrophobic core and headgroup region leading to minimal exchange with bulk solvent, helical content that compares very well with that estimated experimentally from FTIR analyses, and stable association of the dimer via residues that include the $I_{659}XXXV_{663}$ motif over the time scale of the simulation.

■ DISCUSSION

In this work, we sought to quantify the oligomeric states and binding energies of the Neu and Neu* TM domains and two disruptive mutants to more fully interpret previous results obtained in *E. coli* membranes using the TOXCAT assay. To achieve this, we employed simple model systems composed of

dx.doi.org/10.1021/bi201269w | *Biochemistry* 2012, 51, 2558−2568

peptides solubilized in micelles and single-component membranes. The simplicity of these systems has many benefits. Model systems such as these provide a high level of control to the investigator, which aids in the straightforward interpretation of data. We can therefore say with a high degree of confidence that, under the conditions used, both the Neu and the oncogenic Neu* TM domains form strong homodimers. We can also provide, for the first time, standard state free energies of dissociation of 5.53 and 4.41 kcal/mol for the rat Neu and Neu* TM domains, respectively, and demonstrate that the $V_{664}E$ mutation weakens the TM dimer by 1.1 kcal/mol. At the very least, the magnitudes of these free energy values suggest that the TM domain of Neu is the site of strong protein−protein interactions in membrane mimetic systems.

The AUC analyses of a dimerization-disruptive quadruple mutant of the Neu TM domain (Neu_{QM}), originally discovered using the TOXCAT assay[5] and in which both the putative high-affinity $A_{661}XXXG_{665}$ and $I_{659}XXXV_{663}$ motifs are mutated, indicated that this mutant significantly weakens the dimer (by 2.82 kcal/mol) in DPC micelles. However, even in the absence of these interaction sites, there remained some residual helix−helix association, indicating that other residues in the TM domain can play a role in dimerization. This is further supported by results of the MD simulations, which implicate aromatic Phe/Tyr residues as candidates for future investigation. On the basis of the results of HDX in POPC model membranes, we suggest that both the monomeric and dimeric forms of the Neu and Neu_{QM} peptides are almost entirely shielded from exchange with bulk solvent. However, they are not likely to be located entirely within the hydrophobic core of the bilayer because both peptides are approximately 66−67% helical. This roughly translates to a helical region of 22 or 23 amino acids and 10 or 11 nonhelical residues, which probably map onto the ends of the helices. Both the C- and N-termini of the peptides contain positively charged Arg and Lys residues that could associate via electrostatic interactions with the negatively charged phosphate of the phosphatidylcholine headgroup in POPC, holding the nonhelical ends of the peptide within the headgroup region and protecting them from exchange. The MD simulations support this hypothesis. In their dimeric form, these peptides were expected to display positive bilayer mismatch in POPC bilayers that would be offset by the tilting of each helix in the dimer (we reported a tilt angle of <30° based on LD data for wt Neu TM,[5] which agrees with the value obtained in our MD simulation of 24°). We suggest that Neu_{QM} monomers are also tilted to remain buried in the bilayer, as Neu_{QM} displayed similar secondary structure and exchange properties.

Using our model systems, we have also shown that there are several effects operating in concert to bring about changes in the protein−protein and protein−lipid interactions of Neu upon introduction of the oncogenic $V_{664}E$ mutation. First, we have shown that the $V_{664}E$ mutation weakens the TM dimer, but to a lesser degree than the quadruple mutation discussed above, such that there is still a significant dimer population in DPC micelles. The mutation also slightly reduces the helical content in model membranes (the 3.2% difference in helicity reported here accounts for fewer than one amino acid) and increases the tilt angle to >30°.[5] This increased tilt angle is consistent with the reduction in the level of HDX we report here for this peptide. We predict that the Neu* TM domain dimer is more tilted, bringing the polar ends of the peptide even further into the POPC headgroup region and protecting all of them from exchange. More significantly, the $V_{664}E$ mutation limits the modes of interaction (or TM helix orientations) that can stabilize the dimer. We hypothesized previously that the Neu* TM domain contains one predominant dimer arrangement solely reliant on the $I_{659}XXXV_{663}$ motif, which we suggested stabilizes the activated form of the receptor (i.e., leads to oncogenesis).[5] Here we provide strong evidence to support this hypothesis. Mutation of the $I_{659}XXXV_{663}$ motif in Neu* (to create Neu^*_{DM}) yielded a monomeric TM domain peptide, as shown using AUC, suggesting that the $A_{661}XXXG_{665}$ motif is not able to support dimerization in the presence of the $V_{664}E$ mutation. The resulting monomeric TM domain is less tilted and undergoes a transverse shift in the bilayer to exclude E_{664} from the hydrophobic core, as evidenced by the high degree of HDX observed for this peptide (16.3%). This is in reasonable agreement with the piston model proposed by Shahidullah and co-workers,[13] who suggested that the $V_{664}E$ mutation may cause a transverse shift of the Neu TM domain in the bilayer and thus alter the structure and interactions of this domain by placing it in a new chemical environment (e.g., the polar headgroup region). Our data support the spirit of this statement, but in our hands, the single $V_{664}E$ mutation is not sufficient to cause a transverse shift and results in only a slight weakening of the dimer (which does not shift in the membrane). Only once the peptide is mutated and monomeric do we observe the transverse shift. Differences in the experimental conditions or protein constructs used in our study and this previous work, and their effect on monomer−dimer equilibria, may help explain these discrepancies.

Extrapolation of these results to the full-length Neu receptor resident in a highly complex mammalian membrane is a more controversial topic. We previously interpreted our results in terms of the conformational switching or flexible rotation model proposed for RTKs,[19−24] because our results obtained in bacterial membranes[5] and now in micelles and model membranes all suggest that the wt Neu TM domain has at least two stable dimerization modes, while the $V_{664}E$ mutant has only one. However, this interpretation is at variance with recent results. Specifically, in chemical cross-linking experiments conducted with full-length Neu and Neu* proteins, as well as their isolated TM domains, in mammalian membranes it was shown that the $V_{664}E$ mutation led to an increase in both the dimeric form of the receptor and receptor activation,[15,48] thus supporting a model of Neu activation triggered solely by receptor dimerization (and not flexible rotation). Although it is difficult to rule out artifactual cross-linking of hetero-oligomers in the heterogeneous environment of a mammalian membrane in these studies, this dramatic difference in results observed in mammalian membranes versus the DPC micelles and POPC bilayers reported here highlights a fundamental limitation of using pure model systems to study membrane proteins, namely, that one cannot account for the influence of additional lipids and proteins present in the native membrane. It must therefore be considered that the interactions of the Neu TM domain may be greatly altered in the context of the full-length receptor present in its native membrane, because of conformational constraints imposed by other regions of the protein.

■ ASSOCIATED CONTENT

Ⓢ Supporting Information

Additional experimental details for CHI searches and parameters used in molecular dynamic simulations, all CD data collected, results from Gaussian curve fitting of ATR-FTIR spectra (and integrals), and various outputs from the MD simulations of the wt Neu homodimer in a membrane bilayer.

This material is available free of charge via the Internet at http://pubs.acs.org.

AUTHOR INFORMATION

Corresponding Author

*Telephone: +44 2476 150037. Fax: +44 2476 524112. E-mail: ann.dixon@warwick.ac.uk.

Funding

This work was supported by Medical Research Council Grant G0601114 to A.M.D. R.N. thanks Advantage West Midlands and HEFCE for provision of a Birmingham Science City Research Alliance Fellowship. A.N. was supported by an Engineering and Physical Sciences Research Council studentship.

Notes

The authors declare no competing financial interest.

ACKNOWLEDGMENTS

We thank J. Crawford for synthesis of peptides and A. Rodger for use of CD instrumentation. A.N. and R.N. acknowledge the use of computing facilities at the University of Warwick Centre for Scientific Computing.

ABBREVIATIONS

AUC, analytical ultracentrifugation; ATR-FTIR, attenuated total internal reflection Fourier transform infrared spectroscopy; CD, circular dichroism; MD, molecular dynamics; rmsd, root-mean-square deviation; RTK, receptor tyrosine kinase; SDS−PAGE, sodium dodecyl sulfate−polyacrylamide gel electrophoresis; TM, transmembrane.

REFERENCES

(1) Bargmann, C. I., Hung, M. C., and Weinberg, R. A. (1986) Multiple independent activations of the Neu oncogene by a point mutation altering the transmembrane domain of p185. *Cell 45*, 649−657.

(2) Bargmann, C. I., and Weinberg, R. A. (1988) Increased tyrosine kinase activity associated with the protein encoded by the activated Neu oncogene. *Proc. Natl. Acad. Sci. U.S.A. 85*, 5394−5398.

(3) Bargmann, C. I., and Weinberg, R. A. (1988) Oncogenic activation of the Neu-encoded receptor protein by point mutation and deletion. *EMBO J. 7*, 2043−2052.

(4) Weiner, D. B., Liu, J., and Greene, M. I. (1989) A point mutation in the neu oncogene mimics ligand induction of receptor aggregation. *Nature 339*, 230−231.

(5) Beevers, A. J., Damianoglou, A., Oates, J., Rodger, A., and Dixon, A. M. (2010) Sequence-dependent oligomerization of the Neu transmembrane domain suggests inhibition of "conformational switching" by an oncogenic mutant. *Biochemistry 49*, 2811−2820.

(6) Beevers, A. J., and Kukol, A. (2006) The transmembrane domain of the oncogenic mutant ErbB-2 receptor: A structure obtained from site-specific infrared dichroism and molecular dynamics. *J. Mol. Biol. 361*, 945−953.

(7) Houliston, R. S., Hodges, R. S., Sharom, F. J., and Davis, J. H. (2003) Comparison of proto-oncogenic and mutant forms of the transmembrane region of the Neu receptor in TFE. *FEBS Lett. 535*, 39−43.

(8) Houliston, R. S., Hodges, R. S., Sharom, F. J., and Davis, J. H. (2004) Characterisation of the proto-oncogenic and mutant forms of the transmembrane region of Neu in micelles. *J. Biol. Chem. 279*, 24073−24080.

(9) Khemtemourian, L., Buchoux, S., Aussenac, F., and Dufourc, E. J. (2007) Dimerization of Neu/erb2 transmembrane domain is controlled by membrane curvature. *Eur. Biophys. J. 36*, 107−112.

(10) Khemtemourian, L., Lavielle, S., Bathany, K., Schnmitter, J. M., and Dufourc, E. J. (2006) Revisited and large-scale synthesis and purification of the mutated and wild type Neu/ErbB-2 membrane-spanning segment. *J. Pept. Sci. 12*, 361−368.

(11) Smith, S. O., Smith, C. S., Shekar, S., Peersen, O., Ziliox, M., and Aimoto, S. (2002) Transmembrane interactions in the activation of the Neu receptor tyrosine kinase. *Biochemistry 41*, 9321−9332.

(12) Smith, S. O., Smith, C. S., and Bormann, B. J. (1996) Strong hydrogen bonding interactions involving a buried glutamic acid in the transmembrane sequence of the Neu/ErbB-2 receptor. *Nat. Struct. Biol. 3*, 252−258.

(13) Shahidullah, K., Krishnakumar, S. S., and London, E. (2010) The effect of hydrophilic substitutions and anionic lipids upon the transverse positioning of the transmembrane helix of the ErbB2 (neu) protein incorporated into model membrane vesicles. *J. Mol. Biol. 396*, 209−220.

(14) Mendrola, J. M., Berger, M. B., King, M. C., and Lemmon, M. A. (2002) The single transmembrane domains of ErbB receptors self-associate in cell membranes. *J. Biol. Chem. 277*, 4704−4712.

(15) He, L., Shobnam, N., and Hristova, K. (2011) Specific inhibition of a pathogenic receptor tyrosine kinase by its transmembrane domain. *Biochim. Biophys. Acta 1808*, 253−259.

(16) Russ, W. P., and Engelman, D. M. (1999) TOXCAT: A measure of transmembrane helix association in a biological membrane. *Proc. Natl. Acad. Sci. U.S.A. 96*, 863−868.

(17) Sternberg, M. J. E., and Gullick, W. J. (1990) A sequence motif in the transmembrane region of growth-factor receptors with tyrosine kinase activity mediates dimerization. *Protein Eng. 3*, 245−248.

(18) Russ, W. P., and Engelman, D. M. (2000) The GxxxG motif: A framework for transmembrane helix-helix association. *J. Mol. Biol. 296*, 911−919.

(19) Bell, C. A., Tynan, J. A., Hart, K. C., Meyer, A. N., Robertson, S. C., and Donoghue, D. J. (2000) Rotational coupling of the transmembrane and kinase domains of the Neu receptor tyrosine kinase. *Mol. Biol. Cell 11*, 3589−3599.

(20) Schlessinger, J. (2000) Cell signaling by receptor tyrosine kinases. *Cell 103*, 211−225.

(21) Seubert, N., Royer, Y., Staerk, J., Kubatzky, K. F., Moucadel, V., Krishnakumar, S., Smith, S. O., and Constantinescu, S. N. (2003) Active and inactive orientations of the transmembrane and cytosolic domains of the eErythropoietin receptor dimer. *Mol. Cell 12*, 1239−1250.

(22) Yu, X., Sharma, K. D., Takahashi, T., Iwamoto, R., and Mekada, E. (2002) Ligand-independent dimer formation of epidermal growth factor receptor (EGFR) is a step separable from ligand-induced EGFR signaling. *Mol. Biol. Cell 13*, 2547−2557.

(23) Moriki, T., Maruyama, H., and Maruyama, I. N. (2001) Activation of preformed EGF receptor dimers by ligand-induced rotation of the transmembrane domain. *J. Mol. Biol. 311*, 1011−1026.

(24) Fleishman, S. J., Schlessinger, J., and Ben-Tal, N. (2002) A putative molecular-activation switch in the transmembrane domain of ErbB2. *Proc. Natl. Acad. Sci. U.S.A. 99*, 15937−15940.

(25) Hong, H., and Bowie, J. U. (2011) Dramatic destabilization of transmembrane helix interactions by features of natural membrane environments. *J. Am. Chem. Soc. 133*, 11389−11398.

(26) Kauppinen, J. K., Moffatt, D. J., Mantsch, H. H., and Cameron, D. G. (1981) Fourier self-deconvolution: A method for resolving intrinsically overlapped bands. *Appl. Spectrosc. 35*, 271−276.

(27) Beevers, A. J., and Kukol, A. (2006) Secondary structure, orientation, and oligomerization of phospholemman, a cardiac transmembrane protein. *Protein Sci. 15*, 1127−1132.

(28) Lebowitz, J., Lewis, M. S., and Schuck, P. (2002) Modern analytical ultracentrifugation in protein science: A tutorial review. *Protein Sci. 11*, 2067−2079.

(29) Johnson, M. L., Correia, J. J., Yphantis, D. A., and Halvorson, H. R. (1981) Analysis of data from the analytical ultracentrifuge by nonlinear least-squares techniques. *Biophys. J. 36*, 575−588.

(30) Oates, J., Hicks, M., Dafforn, T. R., DiMaio, D., and Dixon, A. M. (2008) In vitro dimerization of the bovine papillomavirus E5 protein transmembrane domain. *Biochemistry 47*, 8985−8992.

(31) Schuck, P. (2000) Size distribution analysis of macromolecules by sedimentation velocity ultracentrifugation and Lamm equation modelling. *Biophys. J. 78*, 1606−1619.
(32) Adams, P. D., Arkin, I. T., Engelman, D. M., and Brunger, A. T. (1995) Computational searching and mutagenesis suggest a structure for the pentameric transmembrane domain of phospholamban. *Nat. Struct. Biol. 2*, 154−162.
(33) Chothia, C., Levitt, M., and Richardson, D. (1981) Helix to helix packing in proteins. *J. Mol. Biol. 145*, 215−250.
(34) Jones, D. H., Ball, E. H., Sharpe, S., Barber, K. R., and Grant, C. W. M. (2000) Expression and membrane assembly of a transmembrane region from Neu. *Biochemistry 39*, 1870−1878.
(35) Rath, A., Glibowicka, M., Nadeau, V. G., Chen, G., and Deber, C. M. (2009) Detergent binding explains anomalous SDS-PAGE migration of membrane proteins. *Proc. Natl. Acad. Sci. U.S.A. 106*, 1760−1765.
(36) Stanley, A. M., and Fleming, K. G. (2005) The transmembrane domains of ErbB receptors do not dimerize strongly in micelles. *J. Mol. Biol. 347*, 759−772.
(37) Fleming, K. G., Ackerman, A. L., and Engelman, D. M. (1997) The effect of point mutations on the free energy of transmembrane α-helix dimerization. *J. Mol. Biol. 272*, 266−275.
(38) Jenei, Z. A., Borthwick, K., Zammit, V. A., and Dixon, A. M. (2009) Self-association of transmembrane domain (TM) 2, but not TM 1, in carnitine palmitoyltransferase 1A: Role of GXXXG(A) motifs. *J. Biol. Chem. 284*, 6988−6997.
(39) Dixon, A. M., Stanley, B. J., Matthews, E. E., Dawson, J. P., and Engelman, D. M. (2006) Invariant chain transmembrane domain trimerization: A step in MHC class II assembly. *Biochemistry 45*, 5228−5234.
(40) Fleming, K. G. (2002) Standardizing the free energy change of transmembrane helix-helix interactions. *J. Mol. Biol. 323*, 563−571.
(41) Duneau, J.-P., Vegh, A. P., and Sturgis, J. N. (2007) A dimerization hierarchy in the transmembrane domains of the HER receptor family. *Biochemistry 46*, 2010−2019.
(42) Rath, P., Bousché, O., Merrill, A. R., Cramer, W. A., and Rothschild, K. J. (1991) Fourier-transform infrared evidence for a predominantly α-helical structure of the membrane-bound channel forming COOH-terminal peptide of Colicin E1. *Biophys. J. 59*, 516−522.
(43) Tatulian, S. A. (2003) Attenuated total reflection Fourier transform infrared spectroscopy: A method of choice for studying membrane proteins and lipids. *Biochemistry 42*, 11898−11907.
(44) Lindahl, E., and Sansom, M. S. P. (2008) Membrane proteins: Molecular dynamics simulations. *Curr. Opin. Struct. Biol. 18*, 425−431.
(45) Samna Soumana, O., Garnier, N., and Genest, M. (2008) Insight into the recognition patterns of the ErbB receptor family transmembrane domains: Heterodimerization models through molecular dynamics search. *Eur. Biophys. J. Biophys. Lett. 37*, 851−864.
(46) Aller, P., Voiry, L., Garnier, N., and Genest, M. (2005) Molecular dynamics (MD) investigations of preformed structures of the transmembrane domain of the oncogenic neu receptor dimer in a DMPC bilayer. *Biopolymers 77*, 184−197.
(47) Beevers, A. J., and Kukol, A. (2006) Systematic molecular dynamics searching in a lipid bilayer: Application to the glycophorin A and oncogenic ErbB2 transmembrane domains. *J. Mol. Graphics Modell. 25*, 226−233.
(48) He, L., and Hristova, K. (2008) Pathogenic activation of receptor tyrosine kinases in mammalian membranes. *J. Mol. Biol. 384*, 1130−1142.